Nano Research 2016, 9(3): 703–712
DOI 10.1007/s12274-015-0949-x
Research Article
ISSN 1998-0124
CN 11-5974/O4

Influence of dielectrics with light absorption on the photonic bandgap of porous alumina photonic crystals

Guoliang Shang, Guangtao Fei (✉), Yue Li, and Lide Zhang

Key Laboratory of Materials Physics and Anhui Key Laboratory of Nanomaterials and Nanostructures, Institute of Solid State Physics, Hefei Institutes of Physical Science, Chinese Academy of Sciences, P. O. Box 1129, Hefei 230031, China

Received: 14 July 2015
Revised: 16 November 2015
Accepted: 21 November 2015

KEYWORDS
photonic crystals,
porous materials,
light–mater interaction,
capillary condensation,
nanotechnology

ABSTRACT

In this work, the influences of dielectrics with light absorption on the photonic bandgaps (PBGs) of porous alumina photonic crystals (PCs) were studied. Transmittance spectra of porous alumina PCs adsorbing ethanol showed that all the PBGs positions red-shifted; however, the transmittance of the PBG bottom showed different trends when the PBGs were located in different wavelength regions. In the near infrared region, liquid ethanol has strong light absorption, and, with the increase in adsorption, the PBG bottom transmittance of porous alumina PCs first increased and then decreased. However, in the visible light region, liquid ethanol has little light absorption, and thus, with the increase in adsorption, the PBG bottom transmittance of porous alumina PCs increased gradually all the time. Simulated results were consistent with the experimental results. The capillary condensation of organic vapors in the pores of porous alumina accounted for the change in the PBG bottom transmittance. The non-negligible light absorption of the organic vapors was the cause of the decrease in the transmittance. The results for porous alumina PC adsorbing methanol, acetone, and toluene further confirmed the influences of light absorption on the PBG bottomed transmittance.

1 Introduction

The interaction between incident light and matter in photonic crystals (PCs) [1, 2] can lead to various phenomena, so changes in the characteristics of materials depend on differences in light–matter interactions [3–9].

A porous alumina-based PC is composed of alternating layers with different porosities and has a large specific surface area [10–12]. One of the unique optical features of PCs is the propagation inhibition of incident light, which is known as a photonic bandgap (PBG). Generally, the bandgap position, bandwidth, and gap to midgap ratio are the main parameters to characterize the properties of the forbidden gaps of PCs. According to the Bragg equation, the location of

Address correspondence to gtfei@issp.ac.cn

the PBG is related to the effective refractive index and thickness of each layer. In porous alumina PCs, changing the effective refractive index, diameter, and length of the alumina holes can lead to variations in the PBG position [12–18]. Therefore, substances in the pores can lead to change in the effective refractive index of each layer and result in a change in the PBG position, which is promising for applications in novel sensors [12–17]. However, researchers mainly focus on the real part of the refractive index during the adsorption of volatile organic compounds (VOCs); in other words, they usually ignore the light losses. These assumptions will not induce significant errors in the case of organic gases with very weak light absorption. Nevertheless, the weak light absorption will be amplified because of the enhanced properties of the PBG [8–10]. Thus, photonic bandedge lasers [10] and fluorescence enhancement [19] can be realized. However, when VOCs are adsorbed by porous materials, the capillary condensation (CC) effect may occur [20–27]. If the VOCs have non-negligible light absorption [28–30], they can also have a significant impact on the PBG. Thus, studying the influences of dielectrics with light absorption on the PBG is necessary, especially for introducing dielectrics into porous materials to achieve novel properties [31, 32].

In this work, we studied the interactions between various adsorbates and PCs experimentally and theoretically. It was found that the light absorption of VOCs adsorbed in the holes of porous alumina PCs plays a vital role in the characteristics of the PBG. If the adsorbates have non-negligible light absorption, the transmittance at the bottom of the PBG shows a dramatic decrease when the adsorbate reaches a certain extent in the pores. These findings are of great importance to better understand the light–matter interactions in PCs and broaden the application fields of PCs.

2 Experimental

2.1 Synthesis of alumina PCs with a narrow photonic bandgap

Porous alumina PCs with narrow PBGs were fabricated by anodizing high-purity aluminum foils (99.999%) using a compensation voltage method, which is also described in our previous studies [11, 17, 32]. In detail, for the first period, the applied voltage increased from 23 to 53 V in the form of a quarter-sinusoidal wave within 30 s and then linearly decreased to 23 V within 3 min. From the second period, a step-compensation voltage was introduced. Each period of the voltage waveform was overall higher than the previous one by 0.055 V for the remaining 99 periods. All the anodic oxidations were controlled by a computer program and carried out in a water tank with a constant temperature of 16 ℃. Finally, the remaining aluminum was removed by chemical etching in saturated $CuCl_2$ solution, and the barrier layer was removed with phosphoric acid (3 wt.%) at 40 ℃.

2.2 Adsorption measurement of as-prepared PC

Transmittance spectrum measurements were carried out with a spectrophotometer (CARY 5E) in normal-incidence mode in a wavelength range of 300–2,000 nm. The as-prepared PC was fixed in a sealed quartz cuvette with sufficient liquid VOC at the bottom to produce a saturated ethanol vapor ambiance. The transmittance spectrum of the sample was recorded repeatedly from when the sample was placed in the sealed quartz cuvette with sufficient liquid ethanol until the transmittance spectrum no longer changed. Two adjacent measurements had a time interval of 50 s.

2.3 Characterization of the structure

Morphologies of samples were observed with a field emission scanning electron microscope (FE-SEM, Sirion 200).

3 Results and discussion

Figure 1 shows SEM images, a diagram, and a transmittance spectrum of an as-prepared sample. As shown in Fig. 1(a), the thickness of the sample was about 47 μm. Similar to our previous works [11, 17, 32], the as-prepared samples had stem and branch channels along the pore growth direction. According to effective dielectric theory, the as-prepared sample can be seen as stem (layer I) and branch (layer II) channel layers alternating in space, as shown in Figs. 1(b) and 1(c).

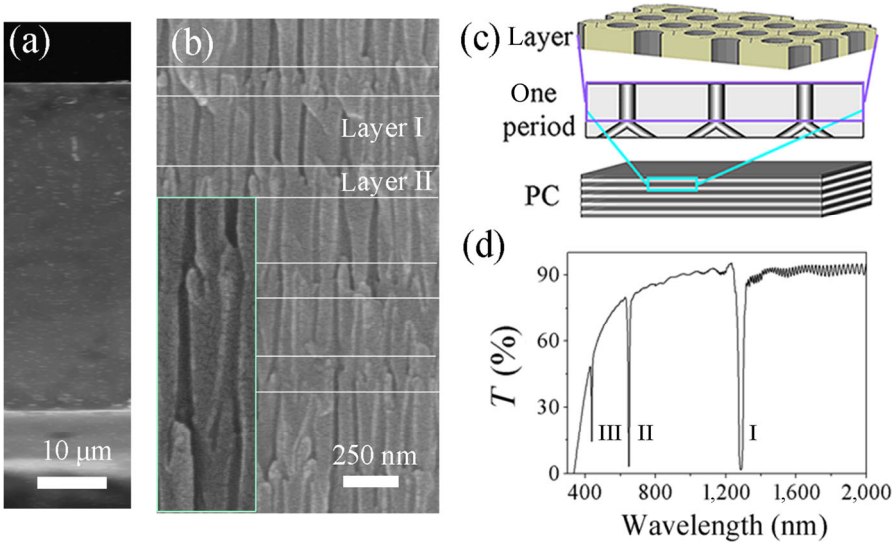

Figure 1 (a) SEM image of the as-prepared porous alumina PC and (b) the enlarged SEM image. Inset is the enlarged SEM of the branched and stem channel. (c) Diagram of the as-prepared sample. (d) Transmittance spectrum of the as-prepared sample. I, II and III denote the three PBGs.

The measured thicknesses of layer I and layer II were about 320 and 140 nm, respectively, and the corresponding pore diameters were 50 and 25 nm, respectively. This type of periodic structure exhibits PBGs along the pore growth direction. As shown in Fig. 1(d), there are three PBGs located at 440 (III), 652 (II), and 1,290 nm (I), and the corresponding full widths at half maximum of the PBGs were 8 (III), 10 (II), and 30 nm (I), respectively. However, the as-prepared PCs were a typical porous material and thus had a large specific surface area and good performances in adsorbing organic molecules. Meanwhile, the intrinsic properties of introduced materials (such as the dielectric constant [12–17], light absorption [27–29], and so on) can affect the characteristics of PBGs significantly.

Figure 2(a) is the transmittance spectra of saturated gaseous ethanol (G-ethanol, dashed line) and liquid ethanol (L-ethanol, solid line) in the visible light region. The shaded region indicates a shift region of the PBG from the position of the PBG before any ethanol was introduced to the position after the PC was saturated with ethanol. In Fig. 2(a), one can see that the transmittance of G-ethanol and L-ethanol both remain at a constant value of ~100%. Figure 2(b) shows the variation in the minimum transmittance of the PBG (denoted as the bottom transmittance) and the position of PBG-II with gradual adsorption of G-ethanol, which demonstrates that the PBG position red-shifted with time. When the adsorption time reached 15 min, the position of PBG-II no longer changed, which indicated that the PCs were saturated by G-ethanol. Meanwhile, the transmittance of the PBG bottom increased gradually and remained almost constant after about 15 min. Figure 2(c) shows the transmittance spectra of G-ethanol and L-ethanol within the infrared region. In this region, the transmittance of G-ethanol remained a constant value of ~100%; however, the transmittance of L-ethanol remained below 80%. Figure 2(d) shows the variation of the bottom transmittance and positions of PBG-I as the sample gradually adsorbed ethanol vapor. The PBG position red-shifted gradually at first, and then no longer changed as the adsorption time was extended to about 16 min. However, the bottom transmittance of PBG-I increased gradually with time and then exhibited a dramatic decrease after about 12 min.

A comparison of Figs. 2(b) and 2(d) shows that the bottom transmittance of the PBGs located in different regions exhibited clearly different trends, which should be considered. To gain physical insight into the transmittance decrease shown in Fig. 2(d), simulations were performed. For a one-dimensional PC at normal incidence, the PBG position λ_m can be derived from the Bragg equation, Eq. (1) [13, 15], and the transmittance T_N of a PC with N periods can be obtained from the

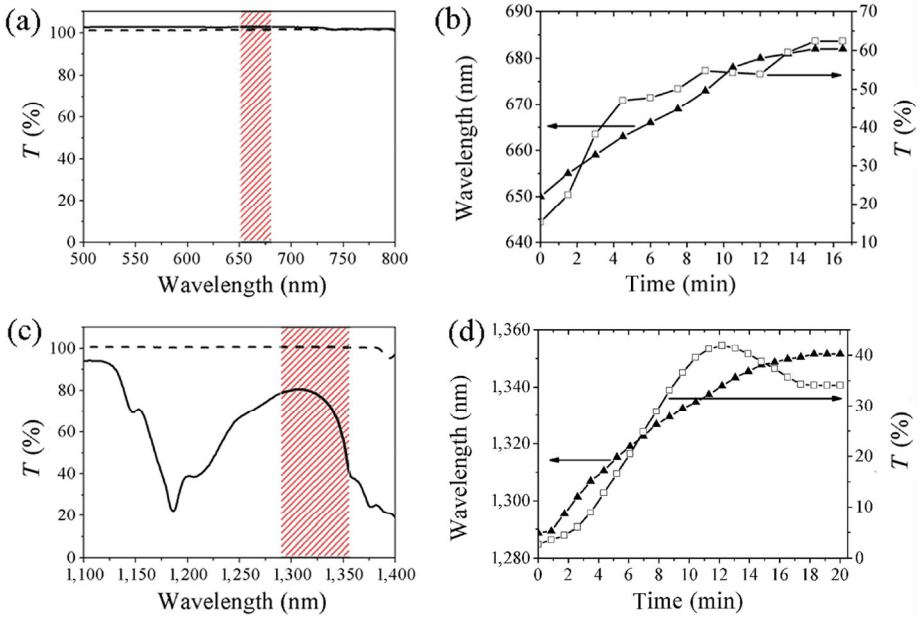

Figure 2 Transmittance spectra of gaseous ethanol (dashed line) and liquid ethanol (solid line) within the visible (a) and near infrared (c) light regions, respectively. (b) and (d) show the bandgap positions (solid triangles) and gap bottom transmittance (transmission minimum of the PBG, hollow squares) of PBGs-II and I changing with adsorption time, respectively. The shaded regions in (a) and (c) indicate the spectral region of the PBG shift from the position of the PBG before any ethanol has been introduced to the position when the PC was saturated with ethanol.

transfer matrix method (TMM, Eq. (2)) [33]

$$\lambda_m = \frac{2}{m}(d_{\mathrm{I}} n_{\mathrm{I}} + d_{\mathrm{II}} n_{\mathrm{II}}) \tag{1}$$

$$\hat{M}_N = (\hat{M}_1)^N = \begin{pmatrix} 1/t_N & r_N^*/t_N^* \\ r_N/t_N & 1/t_N^* \end{pmatrix} \tag{2}$$

where n_{I} and n_{II} are the effective refractive indexes of layer I and layer II, respectively, d_{I} and d_{II} are the corresponding thicknesses, m stands for the diffraction order, M_1 is the transfer matrix of a period, and t_N and r_N are the transmission and reflection parts of a PC with N periods, respectively. The superscript star (*) represents conjugation of the corresponding terms. Herein, we have $|t_N|^2+|r_N|^2 = T_N + R_N = 1$ for a lossless medium, in which T_N and R_N are the transmittance and reflectance, respectively.

Herein, d_{I} and d_{II} can be derived from Fig. 1(b). The porosities of layer I and layer II were estimated to be 50% and 15% based on experimental results, respectively. The volume fraction of alumina ($f_{\mathrm{Al_2O_3}}$) and air (f_{air}) have the relationship $f_{\mathrm{Al_2O_3}} = (1 - f_{\mathrm{air}})$ within a layer. As a result, the corresponding effective dielectric constant ($\varepsilon_{\mathrm{eff}}$) of air-filled pores for layers I and II can be calculated based on the Bruggeman formula (Eq. (3)), which gives the effective dielectric constant of mixture of different dielectrics [34]

$$f_{\mathrm{air}}\left(\frac{\varepsilon_{\mathrm{air}} - \varepsilon_{\mathrm{eff}}}{\varepsilon_{\mathrm{air}} + 2\varepsilon_{\mathrm{eff}}}\right) + f_{\mathrm{Al_2O_3}}\left(\frac{\varepsilon_{\mathrm{Al_2O_3}} - \varepsilon_{\mathrm{eff}}}{\varepsilon_{\mathrm{Al_2O_3}} + 2\varepsilon_{\mathrm{eff}}}\right) = 0 \tag{3}$$

Here, the dielectric constants ($\varepsilon = n^2$, where n is the refractive index) of alumina, air, and ethanol are $\varepsilon_{\mathrm{Al_2O_3}}$ = 2.89, $\varepsilon_{\mathrm{air}}$ = 1, and $\varepsilon_{\mathrm{ethanol}}$ = 1.85. Based on these considerations, the characteristics of the PBG with adsorbed volume fraction of ethanol can be calculated using Eqs. (1)–(3). Since the transmittance of G-ethanol remains at a constant value of about 100% (dotted line in Figs. 2(a) and 2(c)), indicating that there is no light absorption, the effective refractive index of G-ethanol can always be considered as a real value. The PBG variation when the PC adsorbs different volume fractions f of ethanol vapors was simulated, and the results are shown in Fig. 3. Figure 3(a) shows that the PBG had a red shift; meanwhile, the bottom transmittance of the PBG located in visible light region

increased gradually with adsorbed ethanol vapor. In addition, this can be seen intuitively in Fig. 3(b), which was derived directly from Fig. 3(a). Similarly, in the case of PBGs located in the infrared region, the simulated results shown in Figs. 3(c) and 3(d) exhibit the same trend. Compared to Fig. 2, the simulated variation of the PBG is consistent with the experimental results when the PBG is located in the visible light region (Fig. 2(b)) but quite different from the bottom transmittance when the PBGs are located in the infrared region (Fig. 2(d)). Therefore, the simulation results without light absorption could match the experimental results well in the visible light region. However, in the infrared region, the results are deficient. Thus, introduction of light absorption becomes critical for physical insight into the decrease in transmittance.

As is well known, for gaseous materials in porous materials, CC occurs when vapor molecules are adsorbed to a certain extent [19–26]. Since light absorption, represented by k, of L-ethanol cannot be neglected, as indicated in Fig. 2(c), it should also be taken into account [27–29]. When CC occurs, G-ethanol changes to L-ethanol; accordingly, the extinction coefficient k has a dramatic change owing to the dielectric change from gaseous form to liquid form (as shown in Fig. 2(c)). That is, we need to introduce an imaginary part ki into the effective refractive index, where i is the imaginary unit. Herein, the effective refractive index of layer I or layer II with adsorbate in the pores is expressed as $n' = n_{real} + k\mathrm{i}$ for simplification, where n' is the complex refractive index and n_{real} is the real part. Therefore, we adopted the following form for k (see the Electronic Supplementary Material (ESM))

$$k = c \times \mathrm{e}^{f} \tag{4}$$

where c is a constant value. The dramatic change in k expressed by Eq. (4) can indicate the occurrence of CC.

Based on these assumptions, simulation results found by using TMM are given in Fig. 4. The PBG bottom transmittance increased gradually with the f of G-ethanol, as shown in Fig. 4(a), with k in form of Fig. 4(b), herein, $c = 10^{-9}$, and the corresponding k had a magnitude as reported in http://refractiveindex.info. However, the transmittance increased gradually at first and then had a dramatic drop with f, as shown in Fig. 4(c), where k is in form of Fig. 4(d) with $c = 10^{-7}$. Herein, it is believed that the enhancement of light absorption by PC played a significant role in the larger k in the simulation [5–10, 28, 29]. The exhibited

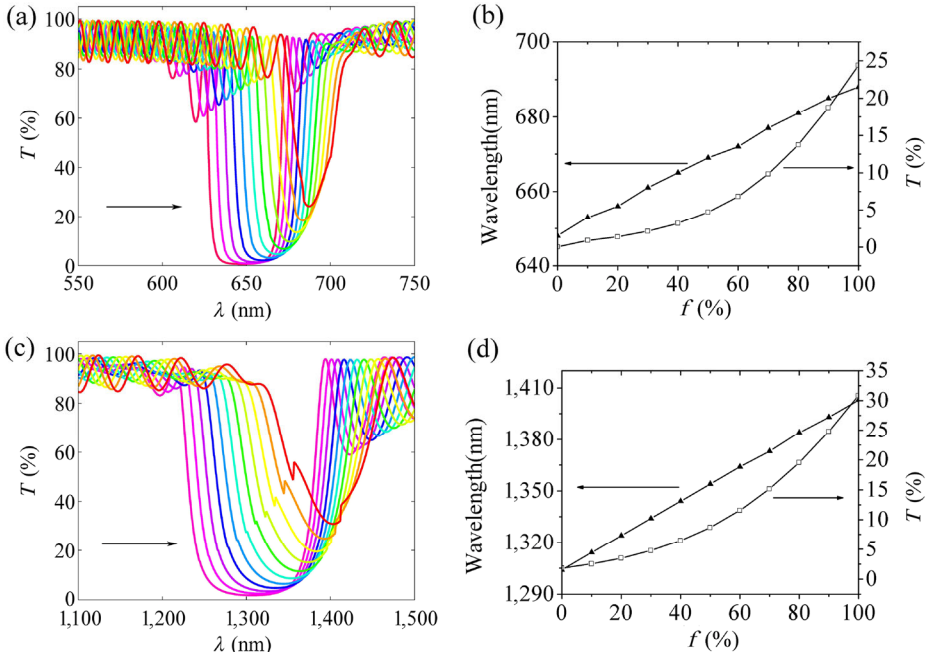

Figure 3 Simulation results of the PC adsorbing different volume fractions (or f, for short) of G-ethanol for a bandgap located in the visible light region ((a) and (b)) and the near-infrared region ((c) and (d)). The step of f is 10%, and $N = 20$ in these simulations. Arrows in (a) and (c) indicate the increase in f of G-ethanol.

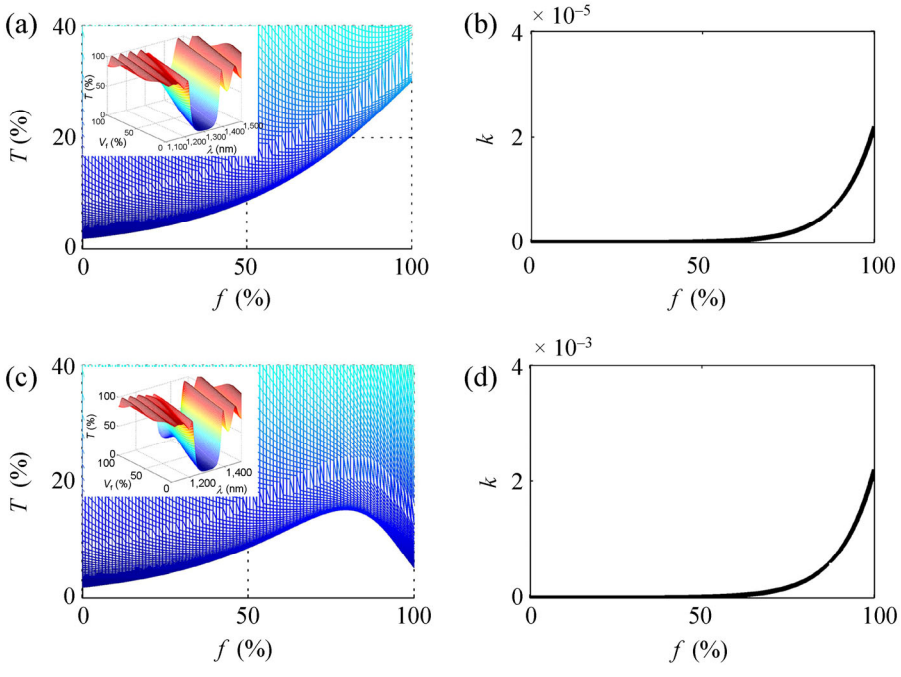

Figure 4 (a) Transmittance of the PBG bottom when the extinction coefficient (k) has the form shown by (b) ($n' = n_{real} + ki$, $k = 10^{-9} \times e^{f}$). (c) Transmittance of the PBG bottom when k has the form shown by (d) ($n' = n_{real} + ki$, $k = 10^{-7} \times e^{f}$). Insets are the corresponding images viewed at different angles.

transmittance decrease is consistent with the experimental result shown in Fig. 2(d).

Additionally, we investigated the influence of k at a constant value of 0, 0.0001, 0.0005, 0.001, 0.003, and 0.01 on PBG, and the corresponding results are shown in Fig. 5. The transmittance of the PBG bottom decreased with k, but the bandwidth increased, as shown in the insets. These results are in good agreement with the previous studies on metallic photonic crystals, in which a super-width PBG appears [28] and light absorption is enhanced [29, 30]. According to all the above results, one possible reason for the decrease in the bottom transmission can be explained as follows. The ethanol vapor is adsorbed gradually by the alumina pores and exists as G-ethanol in the pores initially. Since light absorption of G-ethanol can be neglected (Figs. 2(a) and 2(c)), the transmittance of the PBG bottom increases gradually, as Fig. 3(b) shows. Then, to a certain extent, G-ethanol in the alumina pores changes to a liquid form owing to the CC effect [19–26]. If light absorption of L-ethanol can also be neglected, as shown in Fig. 2(a), the transmittance of the PBG bottom will then also increase (Fig. 2(b)). However, if light absorption of L-ethanol cannot be neglected ($k \neq 0$, as represent in Fig. 2(c)), the transmittance of the PBG bottom will decrease. Therefore, it is reasonable to assume that one possible reason for the decrease in transmittance (Fig. 2(d)) is light absorption, and the turning point may be related to the CC of G-ethanol in alumina pores. A comparison of transmittance changes of PBGs located at different wavelengths indicates that we may observe a phase transition of organic vapors directly just by monitoring the transmittance of a chosen PBG.

According to the above discussion, we believe a decrease in transmittance due to CC is a common phenomenon. Therefore, we systematically studied the relationship between the PBG position (PBG-I) and time when PCs adsorb methanol (Figs. 6(a) and 6(b)), acetone (Figs. 6(c) and 6(d)), and toluene (Figs. 6(e) and 6(f)). Figures 6(a), 6(c), and 6(e) show the transmittance spectra of the gaseous (dashed line) and liquid (solid line) forms of methanol, acetone, and toluene, respectively. The shaded areas represent change ranges of PBG-I when the sample adsorbs different f of those organic vapors. The transmittance of these three types of vapor all remained at a constant value of ~100% within the shaded area. However, the transmittances were different for the liquid forms.

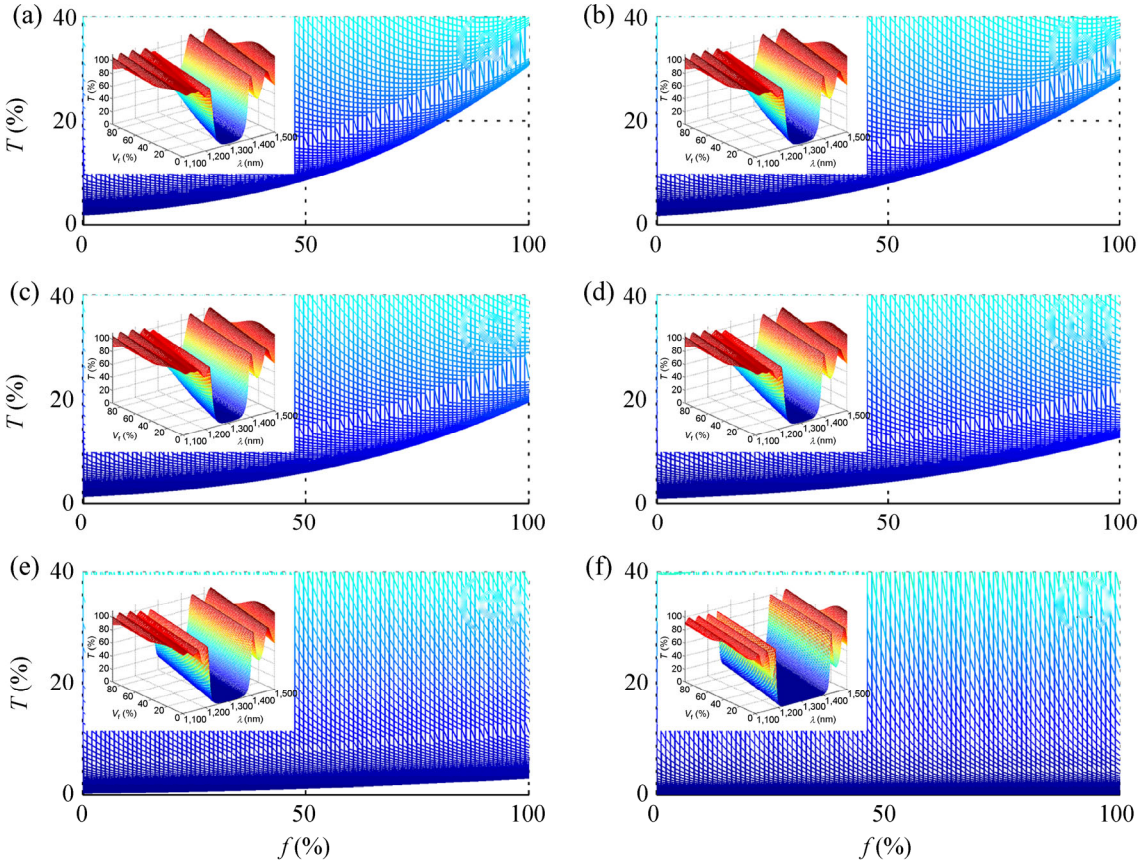

Figure 5 (a)–(f) Simulated transmittance spectra with k of 0, 0.0001, 0.0005, 0.001, 0.003, and 0.01, respectively. The insets are the corresponding three-dimensional images observed at a certain angle.

The bottom transmittance exhibited a dramatic decrease in cases of methanol (Fig. 6(a)) and acetone (Fig. 6(c)), while the variation of the bottom transmittance for toluene (Fig. 6(e)) was much less noticeable. Figs. 6(b), 6(d), and 6(f) show the variation in the PBG positions and gap-bottom transmittance with time. The PBG positions red-shifted for all these vapors. The transmittance shown in Figs. 6(b) and 6(d) had an obvious decrease with time greater than 12 and 5 min, respectively. However, the transmittance in Fig. 6(f) retained an upward trend with time, which is consistent with the simulation results in Fig. 3(a). We think the reason that the minimum in the transmittance spectra for the PCs did not change with the residence time of toluene vapor is that liquid toluene does not absorb light significantly (compared to methanol, ethanol, or acetone) in the 1,300–1,350 nm region. A comparison of all the experiment results in Fig. 6 suggests that the transmittance will have a turning point only when the light transmittance spectra of the vapor and liquid forms are quite different.

Based on all these experimental and simulated results, we believe the turning points of the transmittance when organic vapors are adsorbed by the alumina pores are related to the CC of VOCs. In our experiments, organic vapors (with $k \approx 0$) initially cause a variation in the effective refractive index, thus leading to a red shift of the PBG and a gradual increase in the PBG-bottom transmittance (shown as Figs. 2(b), 2(d), 3(b), 3(d), 4(a), 4(c), 6(b), 6(d), and 6(f)). However, when the volume of organic vapor adsorbed by pores increases to a certain extent, organic vapor liquefies because of the CC effect. If light absorption of gaseous and liquid adsorbates is negligible, the bottom transmittance of the PBG will increase gradually over time (Figs. 2(b), 3(b), 3(d), 4(a), and 6(f)). Otherwise, the transmittance of the PBG bottom will increase gradually and have a dramatic decrease with time (Figs. 2(d), 4(c), 6(b), and 6(d)) when the light absorption of the adsorbates is negligible for the gaseous form but non-negligible for the liquid form.

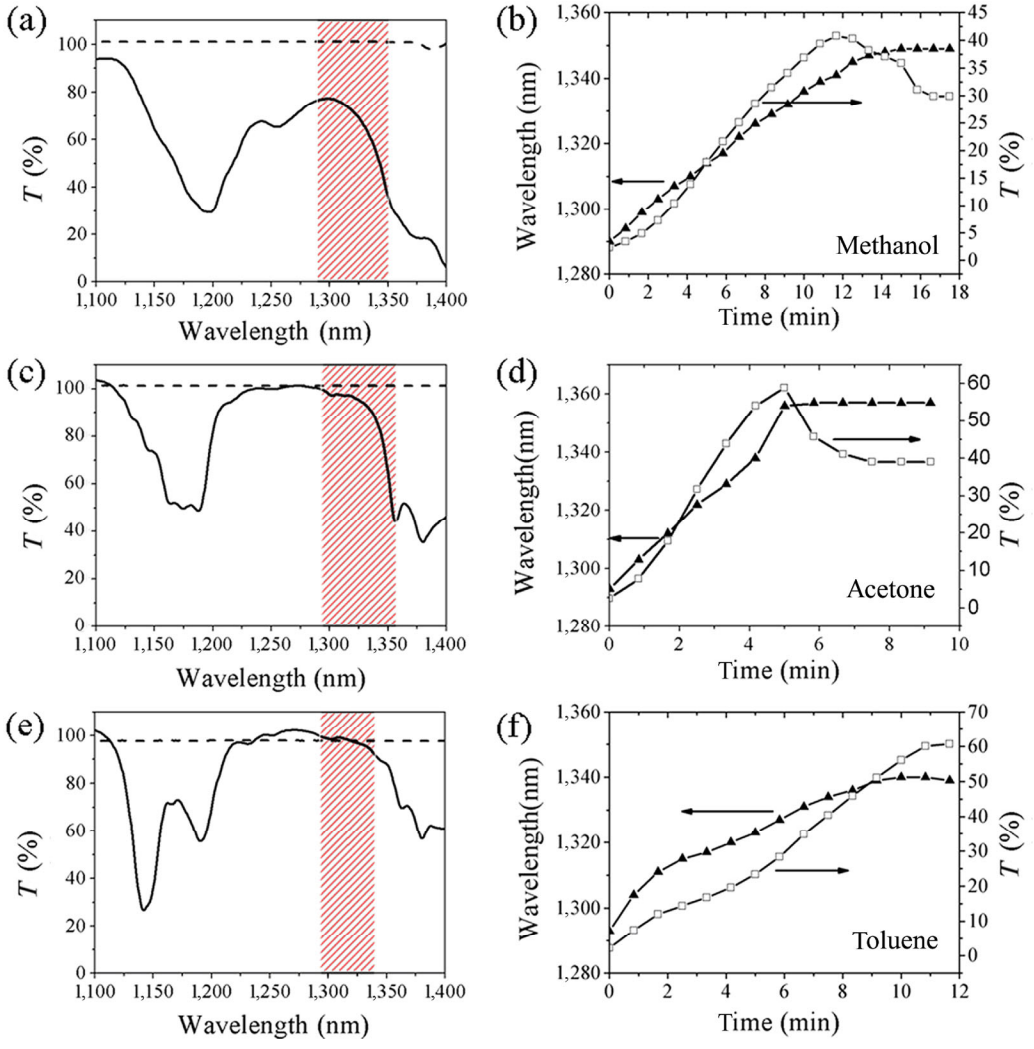

Figure 6 Transmittance spectra of the gas and liquid forms of the analyte, the corresponding PBG, and the transmittance of the PBG bottom with time for methanol ((a) and (b)), acetone ((c) and (d)), and toluene ((e) and (f)), respectively.

4 Conclusions

In this work, we studied interactions between PCs with narrow PBGs and various VOCs (such as ethanol, methanol, acetone, and toluene) adsorbed in the pores of alumina PCs. When the light absorption of gaseous adsorbates is negligible and the counterpart liquid has strong light absorption, the transmittance of the PBG bottom first increases and then decreases with increasing adsorption of organic vapor. However, when the light absorption of the gaseous and liquid adsorbates is negligible, the adsorbates have little impact on the transmittance. Thus, with an increase in adsorption, the transmittance of the PBG bottom increases gradually. The results indicate that the turning point in the gap-bottom transmittance is related to the CC of organic vapor adsorbed by porous alumina pores. These results are helpful to better understand light–matter interactions in PCs, the adsorption and phase transition of organic vapor, and further insight into the kinetics of CC. Furthermore, these findings may have potential applications for *in situ* monitoring the phase change of materials.

Acknowledgements

This work was supported by National Basic Research Program of China (973 Program) (No. 2012CB932303), the National Natural Science Foundation of China (Nos. 51471162, 51171176, and 11404341), and the CAS/SAFEA

International Partnership Program for Creative Research Teams.

Electronic Supplementary Material: Supplementary material (further details of transmittance of the PBG bottom and simulation results of the capillary condensation in porous alumina) is available in the online version of this article at http://dx.doi.org/10.1007/s12274-015-0949-x.

References

[1] Yablonovitch, E. Inhibited spontaneous emission in solid-state physics and electronics. *Phys. Rev. Lett.* **1987**, *58*, 2059–2062.

[2] John, S. Strong localization of photons in certain disordered dielectric superlattices. *Phys. Rev. Lett.* **1987**, *58*, 2486–2489.

[3] Lee, K.; Asher, S. A. Photonic crystal chemical sensors: pH and ionic strength. *J. Am. Chem. Soc.* **2000**, *122*, 9534–9537.

[4] Ruminski, A. M.; King, B. H.; Salonen, J.; Snyder, J. L.; Sailor, M. J. Porous silicon-based optical microsensors for volatile organic analytes: Effect of surface chemistry on stability and specificity. *Adv. Funct. Mater.* **2010**, *20*, 2874–2883.

[5] Ko, D. H.; Tumbleston, J. R.; Zhang, L.; Williams, S.; DeSimone, J. M.; Lopez, R.; Samulski, E. T. Photonic crystal geometry for organic solar cells. *Nano Lett.* **2009**, *9*, 2742–2746.

[6] Guldin, S.; Hüttner, S.; Kolle, M.; Welland, M. E.; Müller-Buschbaum, P.; Friend, R. H.; Steiner, U.; Tétreault, N. Dye-sensitized solar cell based on a three-dimensional photonic crystal. *Nano Lett.* **2010**, *10*, 2303–2309.

[7] Colodrero, S.; Forneli, A.; López-López, C.; Pellejà, L.; Míguez, H.; Palomares, E. Efficient transparent thin dye solar cells based on highly porous 1D photonic crystals. *Adv. Funct. Mater.* **2012**, *22*, 1303–1310.

[8] Dowling, J. P.; Scalora, M.; Bloemer, M. J.; Bowden, C. M. The photonic band edge laser: A new approach to gain enhancement. *J. Appl. Phys.* **1994**, *75*, 1896–1899.

[9] Akahane, Y.; Asano, T.; Song, B. S.; Noda, S. High-Q photonic nanocavity in a two-dimensional photonic crystal. *Nature* **2003**, *425*, 944–947.

[10] Masuda, H.; Yamada, M.; Matsumoto, F.; Yokoyama, S.; Mashiko, S.; Nakao, M.; Nishio, K. Lasing from two-dimensional photonic crystals using anodic porous alumina. *Adv. Mater.* **2006**, *18*, 213–216.

[11] Wang, B.; Fei, G. T.; Wang, M.; Kong, M. G.; Zhang, L. D. Preparation of photonic crystals made of air pores in anodic alumina. *Nanotechnology* **2007**, *18*, 365601.

[12] Guo, D. L.; Fan, L. X.; Wang, F. H.; Huang, S. Y.; Zou, X. W. Porous anodic aluminum oxide Bragg stacks as chemical sensors. *J. Phys. Chem. C* **2008**, *112*, 17952–17956.

[13] Wang, Z. H.; Zhang, J. H.; Xie, J.; Li, C.; Li, Y. F.; Liang, S.; Tian, Z. C.; Wang, T. Q.; Zhang, H.; Li, H. B.; et al. Bioinspired water-vapor-responsive organic/inorganic hybrid one-dimensional photonic crystals with tunable full-color stop band. *Adv. Funct. Mater.* **2010**, *20*, 3784–3790.

[14] Choi, S. Y.; Mamak, M.; von Freymann, G.; Chopra, N.; Ozin, G. A. mesoporous Bragg stack color tunable sensors. *Nano Lett.* **2006**, *6*, 2456–2461.

[15] Shang, G. L.; Fei, G. T.; Zhang, Y.; Yan, P.; Xu, S. H.; Zhang, L. D. Preparation of narrow photonic bandgaps located in the near infrared region and their applications in ethanol gas sensing. *J. Mater. Chem. C* **2013**, *1*, 5285–5291.

[16] Lee, K.; Asher, S. A. Photonic crystal chemical sensors: pH and ionic strength. *J. Am. Chem. Soc.* **2000**, *122*, 9534–9537.

[17] Shang, G. L.; Fei, G. T.; Zhang, Y.; Yan, P.; Xu, S. H.; Ouyang, H. M.; Zhang, L. D. Fano resonance in anodic aluminum oxide based photonic crystals. *Sci. Rep.* **2014**, *4*, 3601.

[18] Joannopoulos, J. D.; Johnson, S. G.; Winn, J. N.; Meade, R. D. *Photonic crystals: Molding the Flow of Light*, 2nd ed.; Princeton University Press: Princeton, 2008.

[19] Zhang, Y. Q.; Wang, J. X.; Ji, Z. Y.; Hu, W. P.; Jiang, L.; Song, Y. L.; Zhu, D. B. Solid-state fluorescence enhancement of organic dyes by photonic crystals. *J. Mater. Chem.* **2007**, *17*, 90–94.

[20] Casanova, F.; Chiang, C. E.; Li, C. P.; Roshchin, I. V.; Ruminski, A. M.; Sailor, M. J.; Schuller, I. K. Gas adsorption and capillary condensation in nanoporous alumina films. *Nanotechnology* **2008**, *19*, 315709.

[21] Bruschi, L.; Mistura, G.; Liu, L. F.; Lee, W.; Gösele, U.; Coasne, B. Capillary condensation and evaporation in alumina nanopores with controlled modulations. *Langmuir* **2010**, *26*, 11894–11898.

[22] Wallacher, D.; Künzner, N.; Kovalev, D.; Knorr, N.; Knorr, K. Capillary condensation in linear mesopores of different shape. *Phys. Rev. Lett.* **2004**, *92*, 195704.

[23] Horikawa, T.; Do, D. D.; Nicholson, D. Capillary condensation of adsorbates in porous materials. *Adv. Colloid Interfac.* **2011**, *169*, 40–58.

[24] Barthelemy, P.; Ghulinyan, M.; Gaburro, Z.; Toninelli, C.; Pavesi, L.; Wiersma, D. S. Optical switching by capillary condensation. *Nat. Photonics* **2007**, *1*, 172–175.

[25] Siderius, D. W.; Shen, V. K. Use of the grand canonical transition-matrix Monte Carlo method to model gas adsorption in porous materials. *J. Phys. Chem. C* **2013**, *117*, 5861–5872.

[26] Kierlik, E.; Monson, P. A.; Rosinberg, M. L.; Sarkisov, L.; Tarjus, G. Capillary condensation in disordered porous materials: Hysteresis versus equilibrium behavior. *Phys. Rev. Lett.* **2001**, *87*, 055701.

[27] Broseta, D.; Barré, L.; Vizika, O.; Shahidzadeh, N.; Guilbaud, J.-P.; Lyonnard, S. Capillary condensation in a fractal porous medium. *Phys. Rev. Lett.* **2001**, *86*, 5313–5316.

[28] Jin, C. J.; Cheng, B. Y.; Man, B. Y.; Zhang, D. Z.; Ban, S. Z.; Sun, B.; Li, L. M.; Zhang, X. D.; Zhang, Z. Q. Two-dimensional metallodielectric photonic crystal with a large band gap. *Appl. Phys. Lett.* **1999**, *75*, 1201–1203.

[29] Hossain, M. M.; Chen, G. Y.; Jia, B. H.; Wang, X. H.; Gu, M. Optimization of enhanced absorption in 3D-woodpile metallic photonic crystals. *Opt. Express* **2010**, *18*, 9048–9054.

[30] Zhang, Z. M.; Du, G. Q.; Jiang, H. T.; Li, Y. H.; Wang, Z. S.; Chen, H. Complete absorption in a heterostructure composed of a metal and a doped photonic crystal. *J. Opt. Soc. Am. B* **2010**, *27*, 909–913.

[31] Sigalas, M. M.; Chan, C. T.; Ho, K. M.; Soukoulis C. M. Metallic photonic band-gap materials. *Phys. Rev. B* **1995**, *52*, 11744–11750.

[32] Shang, G. L.; Fei, G. T.; Xu, S. H.; Yan, P.; Zhang L. D. Preparation of the very uniform pore diameter of anodic alumina oxidation by voltage compensation mode. *Mater. Lett.* **2013**, *110*, 156–159.

[33] Bendickson, J. M.; Dowling, J. P.; Scalora, M. Analytic expressions for the electromagnetic mode density in finite, one-dimensional photonic band-gap structures. *Phys. Rev. E* **1996**, *53*, 4107–4121.

[34] Choy, T. C. *Effective Medium Theory: Principles and Applications*; Oxford University Press: Oxford, 1999.

[35] Casanova, F.; Chiang, C. E.; Li, C. P.; Schuller, I. K. Direct observation of cooperative effects in capillary condensation: The hysteretic origin. *Appl. Phys. Lett.* **2007**, *91*, 243103.